

3D SIMULATION OF FUSING CHARACTERISTICS INCLUDING THE „M-EFFECT“

Manfred Lindmayer ¹

Technische Universität Braunschweig
Institut für Hochspannungstechnik und Elektrische Energieanlagen
Braunschweig, Germany

Abstract: To predict the melting characteristics of fuses by simulation, the combined field problems of current flow in the fuse conductor, and of heat conduction in the complete fuselink are solved using a three-dimensional Finite Volume Method. Additionally, the dissolution of copper in liquid solder, which serves to adjust the characteristics in the low overload region („M-Effect“), is modeled, based on data from furnace measurements of this process. The simulation method allows to predict the local temperature evolution in the fuse, from the adiabatic short-circuit range to the overload region with fusing times in the hour range. Examples are given and compared to measurements. The agreement is good.

1 INTRODUCTION

The time-current characteristic of high-power fuselinks is mainly determined by the geometry of the fuse conductor, the insulating enclosure and the sand filler volume, as well as by their thermal and electrical data (thermal conductivity and capacity, electrical resistivity). Two methods are widely used to adjust the fusing characteristics. Periodic notches in the conductor (current constrictions) determine the near-adiabatic range at high short-circuit currents. The melting- i^2t in this range is directly proportional to the minimum cross-section of the fuse conductor. In time-lag fuses the so-called „M-Effect“ is utilized in the range of low overload current and long fusing times (minute to hour), respectively. A soft solder deposit, generally of tin or tin alloy, in the vicinity of some of the constrictions becomes liquid when a certain overload current is exceeded. It gradually dissolves the fuse conductor of Cu or Ag by diffusion and reduces its cross-section, which in turn leads to further heating until finally melting occurs. This effect shifts the current limit between fusing and non-fusing to lower currents. Related to the same nominal current, M-Effect fuses yield a longer time delay in the overload and short-circuit range, compared to fuses of the same basic design, but without solder.

The adjustment of the fusing characteristic caused by the M-Effect in the overload area depends on many parameters, such as conductor-solder combination, solder volume, conductor thickness and geometry, position of the solder relative to the constrictions, heating intensity in the solder vicinity, and all

other factors that influence the heat balance in the fuse. The new-design of fuses or changes in their characteristics have therefore been a laborious and time-consuming iterative experimental process. Software tools able to model all processes influencing the fusing characteristics could considerably decrease this expenditure.

A realistic simulation has to model the coupled processes of current flow, which determines the local heating power, and of the thermal power balance (= heat diffusion equation), both in a complicated structure consisting of a variety of different materials. Both are described by second order partial differential equations that must be solved by either analytical approximations or numerical methods.

Approaches to simulate these processes have already been made in earlier work. In [1,2,3,4] the temperature distribution, and the thermal and electrical resistances of basic elements of the fuses are described by exact or semi-empirical analytical equations, and combined with iterative solution procedures. In [5] the fuselink is represented by an equivalent R-C network, in [6,7] a similar approach leads to a „transmission line model“. Other simulations discretize the fuselink including its conductor according to Finite Element (FEM) or Finite Difference (FDM) schemes. Because of the typical geometry of fuses a three-dimensional discretization is generally necessary, at least for the heat diffusion problem. In [8,9] a commercial FEM package has been used to model heating of relatively simple fuse geometries without notches and with one single notch, respectively. Other FEM work has been reported in [10,11]. In [12] a 3-dimensional FDM Method, which is similar in principle, was chosen to simulate pre-arcing characteristics.

The dissolution process behind the „M-Effect“ has either not been taken into account in some work, it has been simplified by an „effective melting temperature“ [1], or modeled by a temperature-dependent dissolution speed derived from measurements [8,9]. In [5,13] the basic 2nd order partial differential equation for the local and temporal concentration of Ag in Sn (Fick's second law) has been used. The problem was transferred to an equivalent electric network and solved by a network simulation package. For this the solder and conductor must be finely meshed around the solder spots.

¹ The author is indebted to Messrs. Brogl, Rückling, and Zenkel from Lindner GmbH, Eggolsheim for valuable discussions and for providing measured fuse data.

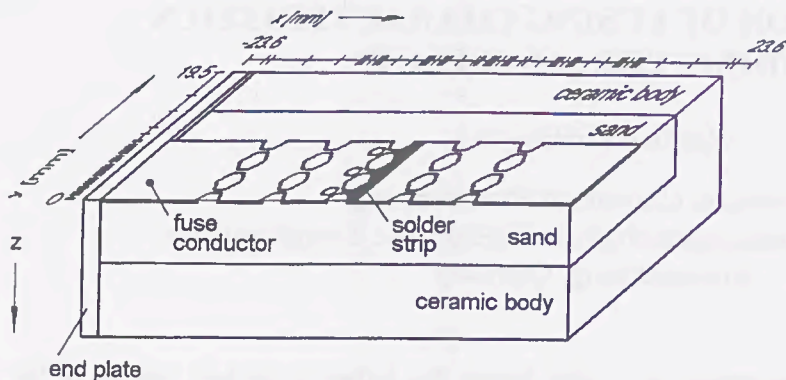


Fig. 1: 3D model of a fuse 100 A, NH 00. (Right end plate removed)

While former work, due to limited computer capabilities, often had to concentrate on partial problems or on parts of the fuse geometry only, the progress in computer technology enables the modeling of more and more complex structures in less time. It has therefore been the aim of this work to develop a Windows-based program code for modeling complete fuses, including the M-Effect, on PCs.

2 FDM SIMULATION METHOD

2.1 Heat Balance (Heat Diffusion)

The starting point is the power balance equation for each volume element dV in the integral formulation

$$\iiint \frac{j^2}{\sigma} dV = \iiint \rho c_p \frac{\partial T}{\partial t} dV - \iiint \text{div}(\lambda \cdot \text{grad } T) dV \quad (1)$$

elec. gener. heat storage thermal conduction

The left term of equ. 1 (it exists only in the fuse conductor elements) denotes the heating power from the current flow. It is in balance with the heat stored by temporal change of temperature, and the power removed from the element by thermal conduction. For steady state temperature calculations the heat storage term is zero. By using Gauss' integral law, the last term is replaced by

$$- \oint (\lambda \cdot \text{grad } T) d\vec{n}, \quad (2)$$

which expresses that the heat conduction term is equivalent to the power that traverses the surface of the volume element.

2.2 Potential Equation and Current Density Distribution

The equation for the electric potential (Laplace equation) is of the same type as equ. 1, but only consists of the conduction term:

$$\iiint \text{div}(\sigma \cdot \text{grad } U) dV = 0 \quad (3a)$$

and

$$\oint (\sigma \cdot \text{grad } U) d\vec{n} = 0, \quad (3b)$$

respectively. When the potential is known from solving equ. 3, the current density j necessary in equ. 1 follows from

$$j_x = \sigma \cdot \partial U / \partial x, \quad j_y = \sigma \cdot \partial U / \partial y, \quad j_z = \dots \quad (4)$$

$$j = \sqrt{j_x^2 + j_y^2 + j_z^2}$$

The calculation of equ. 3 can be restricted to the region of the fuse conductor. If this is a flat strip it could further be simplified two-dimensionally. To allow for more complicated geometries, the 3D representation was kept throughout. In this case it has proved satisfactory to model the complete thickness of the conductor (in Fig. 1 in z -direction) by only one element.

2.3 Discretization

Fig. 1 gives an example of a fuselink with indications of the discretization. The scheme is in principle identical for both field problems. It is also referred to as Finite Volume Method. The complete three-dimensional simulation volume is divided in x -, y -, and z -direction by a rectangular, not necessarily equidistant grid. The grid points are indexed i in x -, k in y - and l in z -direction. Each brick-shaped domain between 8 adjacent grid points has thermal and electrical properties, which are constant within each domain, but dependent on its average temperature, which changes with time. The domains are indexed according to their left, frontal, upper edge point. The temperature equation (equ. 1, 2) and the potential equation (equ. 3), respectively, are set up as difference equations and solved for all grid points. For this the balance over the control volume around each point i, k, l consists of the contributions of the 8 neighbor regions, namely:

i, k, l and $i+1, k, l$ and $i, k+1, l$ and $i, k, l+1$ and $i+1, k+1, l$ and $i+1, k, l+1$ and $i, k+1, l+1$ and $i+1, k+1, l+1$.

The principle can best be seen for the two-dimensional case, Fig. 2, where only the indices i and k are used in x - and y -direction, and where each point i, k shares only 4 neighbor regions. The balance is set up for the area within the dashed lines, which divide each grid distance in two. Further details about the two-dimensional discretization can be seen in [14,15,16]. The three-dimensional procedure is equivalent and yields for each grid point i, k, l a linear equation of the form

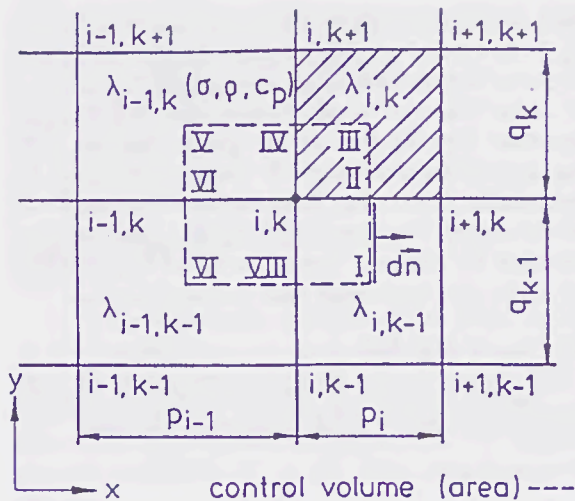


Fig. 2: Discretization (2D).

$$\begin{aligned}
 & -N_{i,k,l} \cdot T_{i,k+1,l} - W_{i,k,l} \cdot T_{i-1,k,l} \\
 & -S_{i,k,l} \cdot T_{i,k-1,l} - E_{i,k,l} \cdot T_{i+1,k,l} \\
 & -G_{i,k,l} \cdot T_{i,k,l+1} - H_{i,k,l} \cdot T_{i,k,l-1} \\
 & + M_{i,k,l} \cdot T_{i,k,l} = D_{i,k,l}
 \end{aligned} \quad (5)$$

This equation links the temperature of point i, k, l (M stands for *Middle* coefficient) to its 6 neighbor points in the directions North, West, South, East, Ground, and Heaven via the appropriate coefficients. Because of symmetry of the problem, e.g. $W_{i,k,l} = E_{i-1,k,l}$, only three sorts of coefficients (N, E, G) are needed for each point. They contain the grid distances and the temperature-dependent properties of the partial volumes. The right-hand side $D_{i,k,l}$ contains the known temperature of point i, k, l at the old time step, the links to neighboring boundary points (if existing), and, if the volume is a conductor element, the heating power j^2/σ integrated over the control volume. The latter results from the current distribution simulation in the conductor.

Equ. 5 for all points constitutes a system of linear equations of the form

$$A \cdot \underline{x} + \underline{b} = 0, \quad (6)$$

where A is a square matrix containing the M, N, E, G links to the neighbors, \underline{x} the vector of the unknown temperatures in the grid points at the new time step, and \underline{b} the vector of known values that result from the boundary points and the temperatures at the last time step as well. As the coefficients of A depend on the temperatures, equ. 6, which is an implicit scheme for the unknown temperatures, must be set up and solved for every time step. (It has proved that the temperature values from the latest time step are accurate enough for this, so iterations of these coefficients within each time step are not necessary.)

2.4 Boundary Conditions

In the potential calculation the Dirichlet condition $U=0$ is taken for the left end plate and $U=1$ V for the right one, while the other boundaries are iso-

lated ($\partial/\partial n = 0$). After integrating the resulting current densities across one of the end plates the voltage drop is corrected linearly to the actual current. The current may be kept constant or vary with time, e.g. sinusoidally. For the work reported here D.C. current was used, yielding directly the virtual melting time.

For the temperature boundaries the outer coordinates of the end plates were assumed to have constant temperature (Dirichlet). To account for the heating by the contact resistance and the current leads [1], temperatures higher than room temperature, e.g. 80 °C, were taken. The outer areas of the ceramic body were treated as heat transmission to the surroundings with $1.2 \cdot 10^6$ Watts per square millimeter and Kelvin of super-temperature. It was found, however, that this has little effect, and that these areas could be regarded as thermally isolating.

Symmetries were taken into account by appropriate symmetry conditions. The example of Fig. 1 represents the complete fuse length in x direction, but it is symmetrical with respect to $y=0$ and $z=0$. (Though the solder layer is applied only one-sided in z direction, the method described in section 3.2, Fig. 5b allows to use symmetry conditions.)

2.5 Computation Procedure

To solve the large equation system (equ. 6) - the thermal model of Fig. 1 consists of approx. 35 000 nodes - a fast iterative solution method with preconditioning [17] was chosen. For simulations of the stationary state the potential/current density simulation and the stationary temperature simulation were carried out alternately with actualized material data at every step, until the results converged. For the simulation of temporal temperature evolution the potential/current density calculation should normally be followed by the next time step of the dynamic temperature calculation, and so on. It was found out that it is sufficient for the usual fuse conductor geometries to compute the current distribution only once at the beginning, despite of the considerably changing temperature and hence electrical conductivity distribution. The current has to flow through the constrictions anyhow, so the current density distribution, especially in the notches where most of the heat is generated, does not vary much.

The dynamic calculation is finished when the melting point in the hottest spot of the conductor is reached.

3 MODEL OF FUSE CONDUCTOR DISSOLUTION IN SOLDER

3.1 Diffusion Data

The dissolution of silver or copper in solder, which becomes appreciable when the liquidus temperature of the solder is exceeded, is a rather complex process, and it has to be more or less simplified. Following Cu and Sn stand also for other combinations of solid metal and solder. Diffusion may be described by Fick's second law [13] for the concentration C (in this

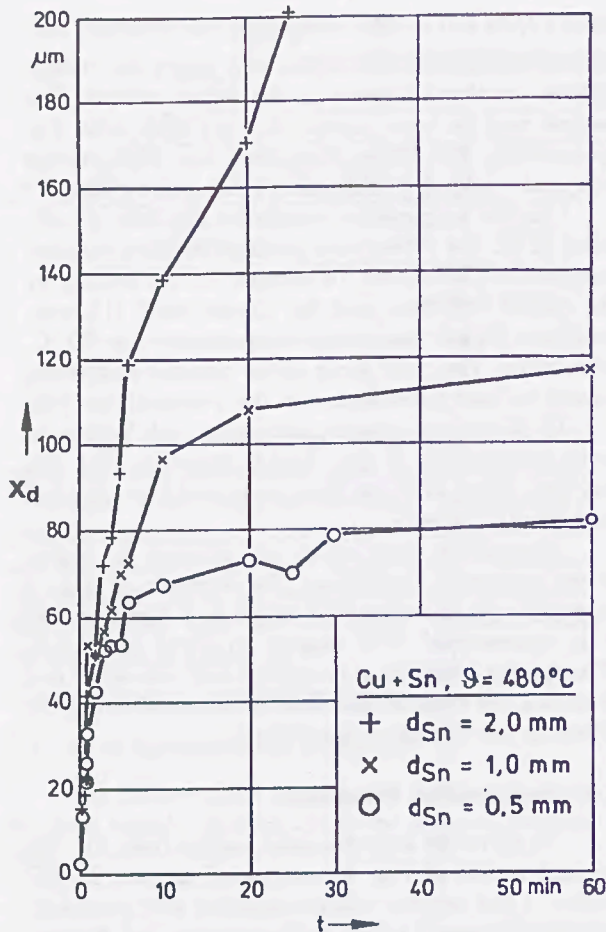


Fig. 3: Mean dissolution depth of Cu in Sn for different solder thickness d_s , $d_{Cu} = 200 \mu\text{m}$, $\theta = 480^\circ\text{C}$.

case the concentration of copper in liquid tin or tin alloy).

$$\frac{\partial C}{\partial t} = D \frac{\partial^2 C}{\partial x^2} \quad (7)$$

The diffusion constant D is temperature-dependent and follows the Arrhenius law.

$$D = D_0 \cdot \exp[-Q / (kT)], \quad (8)$$

where Q is an activation energy.

Equ. 7 also describes the diffusion of liquid Sn into solid Cu, however this process is negligible in comparison [18]. The solution of equ. 7 yields a quadratic increase of dissolution depth with time, which has been observed by some authors [13,19]. Equ. 7, which describes any diffusion process in principle, applied to the diffusion of a solid metal (concentration $C=100\%$) into a liquid metal (solder) would yield an ever increasing concentration and cannot account for the fact that there is clearly a temperature-dependent saturation. Also the exact local gradient of concentration within the solder would play an outstanding role. It has been shown clearly in furnace experiments [8] that the depth of Cu (and Ag, respectively) consumption („dissolution depth“) by liquid Sn or Sn alloy approaches a temperature-dependent saturation value,

which is roughly proportional to the solder thickness, Fig. 3. A detailed consideration in [8] proves that this correlates with the maximum amount of Cu soluble in the liquid Sn, and which follows the temperature-dependent liquidus line of the phase diagram [20], plus an additional amount of copper consumed by intermetallic layers that form between the solid Cu and the solder. The dissolution depth x_d and the concentration by volume C , respectively, of Fig. 3 follow a $[1 - \exp(-t/\tau)]$ curve rather than a square root law:

$$x_d(t) = x_{\text{sat}} \cdot [1 - \exp(-t/\tau)] \quad (9)$$

x_{sat} and τ depend on the temperature θ . The differentiation of equ. 9 yields the dissolution speed:

$$v_d = v_0 \cdot \exp(-t/\tau) \quad (10)$$

This means that the dissolution speed starts with an initial value v_0 and decreases to zero as the final concentration $C_{\text{sat}}(\theta)$ is approached. The simplest and physically sound way to account for this is to assume that the volume concentration of conductor metal in the liquid solder is constant across the molten pool, and that the dissolution speed depends on the concentration ratio

$$v_d(C, \theta) = v_0(\theta) \cdot [1 - C/C_{\text{sat}}(\theta)] \quad (11)$$

The momentary concentration by volume C is related to the dissolution depth x_d by

$$C = x_d / (d_s + x_d) \quad (12)$$

Fig. 4 shows results of $C_{\text{sat}}(T)$ derived from the liquidus line [20] and of $v_0(T)$ measured by [8] in an

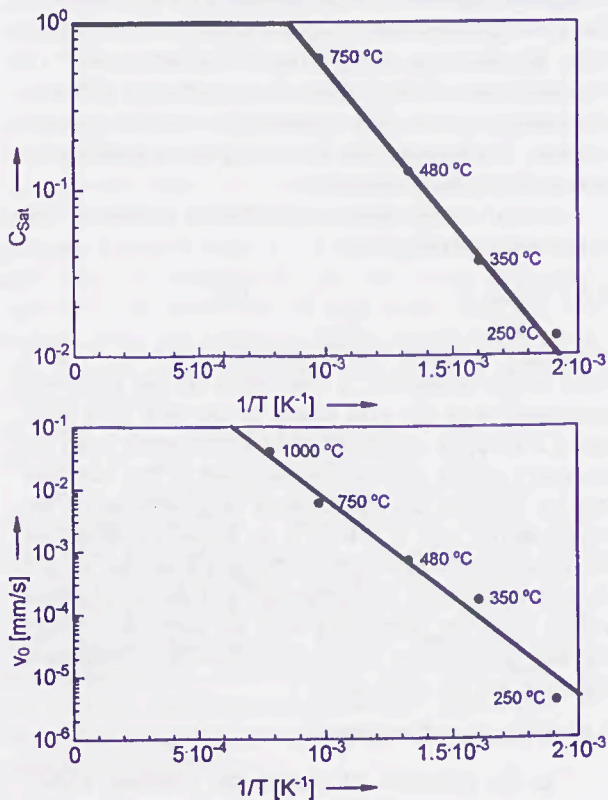


Fig. 4: Saturation concentration C_{sat} and initial dissolution speed v_0 of Cu in liquid Sn.

Arrhenius plot. They can be approximated by

$$C_{Sat} = \max \left\{ \frac{32.8 \cdot \exp\left(\frac{-4150 \text{ K}}{T}\right)}{1} \right\} \quad (13)$$

$$\frac{v_0}{\text{mm/s}} = 155 \cdot \exp\left(\frac{-7640 \text{ K}}{T}\right) \quad (14)$$

In the subsequent simulations the factor in equ. 13 was doubled, i.e. 65.6 instead of 32.8, because this gave the best correlation with measurements. This is physically justified because the additional consumption of Cu by intermetallic layers (at lower temperatures up to 100% [8]) is not taken into account by equ. 13.

3.2 Implementation into FDM Model

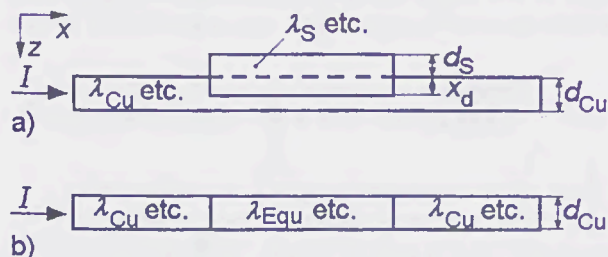


Fig. 5: Replacement of conductor/solder sandwich by an equivalent conductor.

a) original sandwich b) equivalent

The assumption of a concentration C independent of the local position within the solder pool enables the simplification in z direction illustrated in Fig. 5. Instead of a complete discretization across the conductor/solder sandwich, this cross-section is replaced by an equivalent conductor of the original thickness d_{Cu} , but with equivalent data for the electrical and thermal conductivity, such as

$$\lambda_{Equ} = \frac{\lambda_{Cu}(d_{Cu} - x_d) + \lambda_S(d_S + x_d)}{d_{Cu}}, \quad (15)$$

i.e. both parts are switched parallel and concentrated into one equivalent conductor. This is justified because the current flows mainly perpendicular to the z direction and the temperature difference across the sandwich thickness is only small. The data of λ , σ for the solder vary with the solder composition and are not known. It was found out by comparison be-

tween simulations and measurements, however, that the best approximation is to assume them to be negligibly low. Then the electrical and thermal transport is only determined by the remaining copper thickness. This seems justified, too, because the conductivities of liquid solder and of intermetallic Cu-Sn compounds are known to show low values compared with the base metal. The heat capacity of the solder is treated accordingly, but not neglected.

The dissolution depth x_d at each time step and each solder location is calculated by adding $\Delta t \cdot v_d$ to the x_d values accumulated during the previous time steps. v_d follows from equ. 11.

4 SIMULATION EXAMPLES AND COMPARISON WITH MEASUREMENTS

4.1 Fuse Models

As an example Fig. 6 shows a section of the 100 A fuse conductor of Fig. 1. Due to symmetry only one half of the six parallel rows of constrictions is modeled in y direction. If the effect of the sand and the ceramic part lying outside the conductor geometry in y direction could be neglected, it would have been sufficient to model only a small disc-shaped portion (1/12) of the complete fuse between $y = 0$ and the dashed line. The trapezoidal notches (neck width 0.5 mm, length 1 mm) plus the additional round heating holes are replaced by step-shaped contours. The hatched area covered by solder extends over a multitude of elements, thus enabling the local resolution of the Cu dissolution process.

In order to model the adiabatic range at high currents correctly, the heat capacity of the z layer adjacent to the conductor layer (whose thickness is half of the conductor thickness of ≈ 0.15 mm) should not add much to the resulting heat capacity of the relevant nodes. This means that the thickness of the first sand layer has to be small [21], e.g. < 0.1 mm. The thickness of the following layers is increased gradually.

There are in principle many ways to fit the simulation data to measurements, especially the data of solder dissolution. For the electrical resistivity, heat conductivity and heat capacity of the Cu conductor and the ceramic body standard data from the literature were taken, with a first order dependence on temperature. The data for sand are based on measurements in [8]. Depending on the sand quality the heat conductivity ranged between 0.27 and 0.4 W/(m·K), with a temperature coefficient between $1.26 \cdot 10^{-3}$ and $1.37 \cdot 10^{-3} \text{ K}^{-1}$. Due to the best agreement the lower

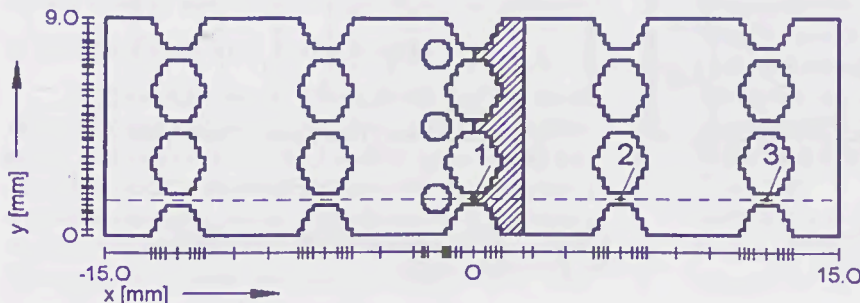


Fig. 6: Section of the fuse conductor of Fig. 1. Dashed Line: Temperature path for Fig. 8

values were taken. The specific heat was taken as $0.6 \text{ Ws}/(\text{g}\cdot\text{K})$, with a temperature coefficient of $1.7 \cdot 10^{-3} \text{ K}^{-1}$ [8]. The solder diffusion was modeled with the data from section 3.1.

4.2 Simulation Results

The simulation yields the temporal evolution of electric potential, current density, and temperature at any point. The following typical results were gained for the fuse of Fig. 1, Fig. 6 with a deposit of solder 0.6 mm thick.

Fig. 7 depicts the simulated evolution of the temperatures as well as the solder dissolution depth with three currents that are typical for different regimes. In Fig. 8 the temperature profiles when the hottest spot just reaches melting temperature are shown for these cases.

At $1.6 \cdot I_n$ the solder dissolution is the governing mechanism. The solder dissolution starts slowly when the solder melting point is exceeded. The temperatures

after an initial rise to nearly stationary conditions increase only slowly due to the decreasing Cu thickness. (Without solder the hottest point, position 1, would reach a stationary temperature of around $350 \text{ }^\circ\text{C}$.) Finally, when most of the copper thickness has been consumed, the situation tilts. The temperature approaches quickly the melting point in the central constrictions with the solder deposit, the complete Cu thickness is being diffused through in these spots. Except for the sharp peak resulting from the final heating, the temperature profile (Fig. 8) shows a continuous drop from the center to the end plates

At $25 \cdot I_n$ on the other hand, the heating process is nearly adiabatic. All constrictions - except for the central ones (position 1), whose heat capacity is higher due to the solder - show an identical progressive temperature rise until they melt after a few milliseconds. The profile clearly shows that the heat generated in the necks has not diffused outward yet. The solder dissolution in this short time is practically zero.

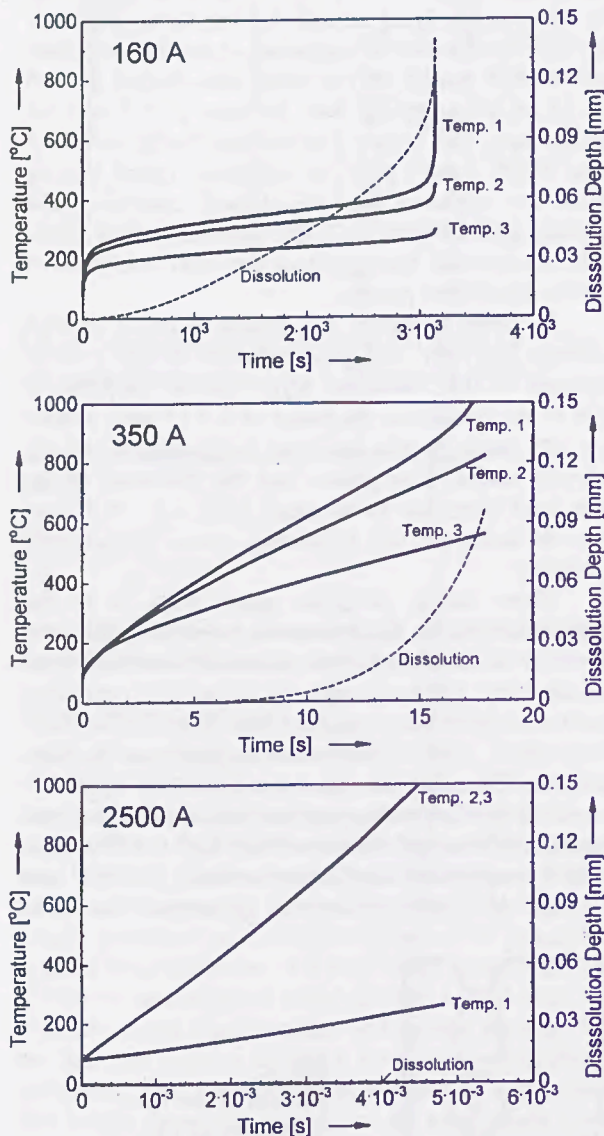


Fig. 7: Temporal evolution of temperature at different points and dissolution depth at point 1 for different currents.

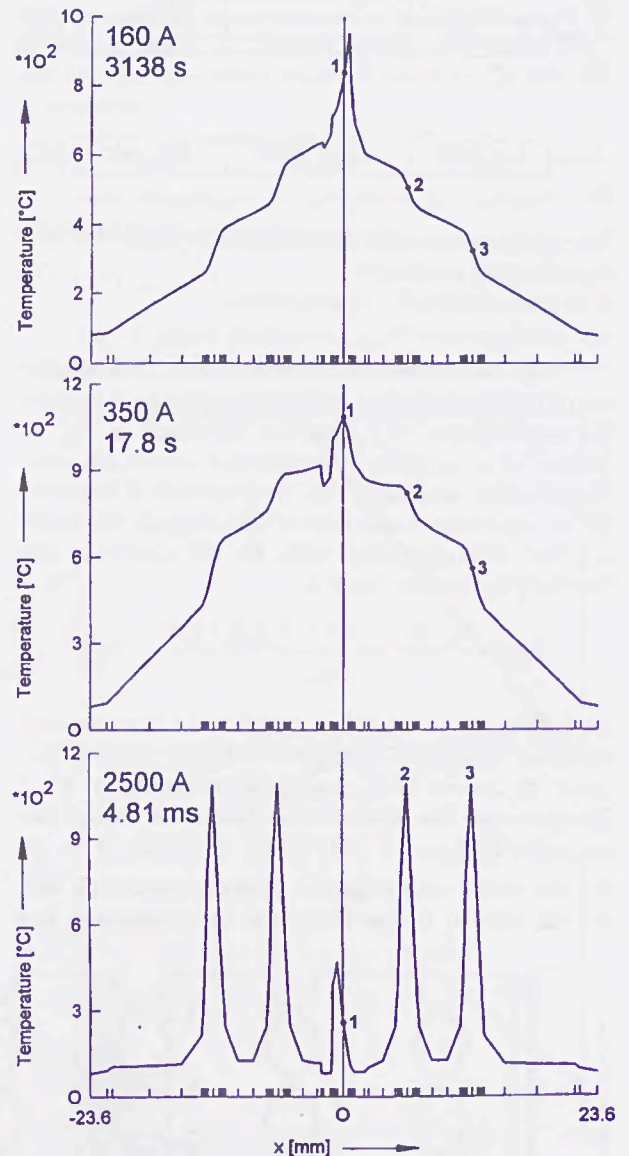


Fig. 8: Temperature profiles on melting for different currents.

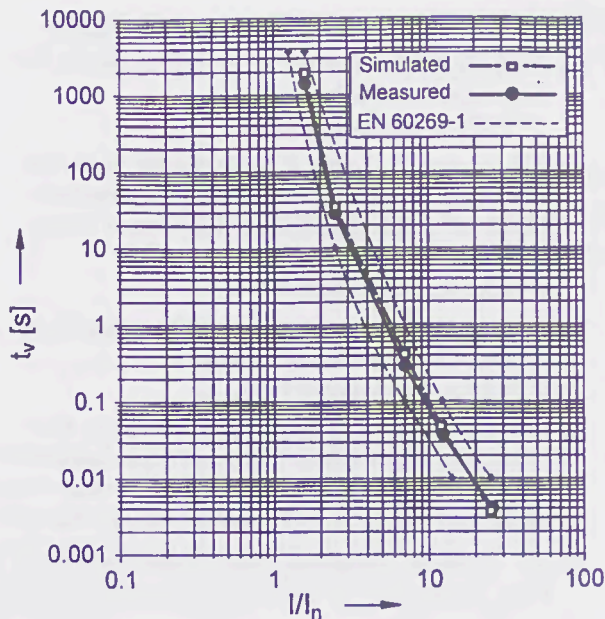


Fig. 9: Comparison of simulated and measured fusing characteristics. 50 A Fuse NH 00, gG.

The current $3.5 \cdot I_n$ with a fusing time of the order of 20 seconds is an intermediate condition where the solder dissolution just begins to play a role. The time scale is long enough for the heat to diffuse out of the constrictions, but still far from near-stationary. The dissolution depth at the moment of melting has reached about $2/3$ of the total conductor thickness, the reduced copper cross-section has already contributed to some additional heating. The peak in the temperature profile in the center is also an indication of this. A comparison with Fig. 10 shows that in this current range the time-current characteristic begins to deviate from that of an identical fuse without solder.

Fig. 9 compares time-current characteristics of simulations and measurements of a 50 A fuse. It has three parallel rows of necks with similar main dimensions as those of Fig. 1/ Fig. 6. The dashed lines mark the region determined by EN 60269-1 / IEC 269-1. The good agreement, which was also found for fuses with other rated currents, confirms the usefulness of the simulation method as a tool for fuse design.

To demonstrate the influence of the „M-Effect“ on the fusing characteristic, Fig. 10 shows a comparison with an additional simulation, where the solder has been removed. The fusing characteristics are identical for $I/I_n \geq 4$. Below this threshold the dissolution process becomes effective and shifts the characteristic towards lower currents and times, respectively.

5 SUMMARY AND CONCLUSION

A three-dimensional FDM model for the simulation of fuses has been presented, including a model of the dissolution of the fuse conductor in liquid solder („M-Effect“). It simplifies the diffusion process by a dissolution speed, which depends on the temperature and the concentration of conductor metal in the solder. Examples of typical simulation results have been

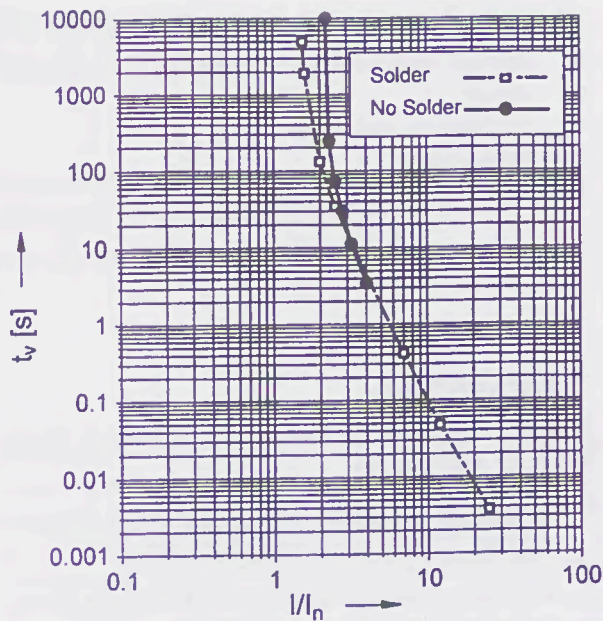


Fig. 10: Simulated pre-arcing times without solder and with solder.

presented and discussed. The good agreement between simulated and measured time-current characteristics confirms the usefulness of the simulation method as a design tool.

6 LIST OF SYMBOLS

A	coefficient matrix
b	vector of known quantities
C	concentration (by volume)
C_{Sat}	saturation concentration
c_p	specific heat
D, D_0	diffusion constant
d_{Cu}	thickness of (Cu) conductor
d_s	thickness of solder layer
$d\vec{n}$	element of surface area
dV	volume element
I	current
I_n	rated current
i, k, l	indices
k	Boltzmann constant
j	current density
t	time
Q	activation energy
T	absolute temperature
t_v	virtual melting time
U	voltage, electric potential
v_d	dissolution speed
v_0	initial dissolution speed
x, y, z	Cartesian coordinates, directions
x_d	dissolution depth
x_{Sat}	saturation dissolution depth
\underline{x}	vector of unknown temperatures (potentials)
D, E, G, H, M, S, W	coefficients of difference equation
Δt	time increment
λ	thermal conductivity

- λ_{Cu} thermal conductivity of (Cu) conductor
 λ_s thermal conductivity of solder
 ρ density
 σ electrical conductivity
 ϑ temperature
 τ time constant

7 REFERENCES

ICEFA = International Conference on Electric Fuses and their Applications.

- 1 R. Wilkins: Simulation of Fuselink Temperature-Rise Tests. 2nd ICEFA, Trondheim 1984.
- 2 R. Wilkins: Steady-State Current Sharing in Fuses with Assymmetrical Arrangements. 4th ICEFA, Nottingham 1991.
- 3 M. Laurent, P. Schaditzki: Fuse-Element - Ageing and Modeling. 3rd ICEFA, Eindhoven 1987.
- 4 J.G.J. Sloot: Analog Simulations of the Heat Flow in a High Voltage Fuse. 3rd ICEFA, Eindhoven 1987.
- 5 D.A. Beaujean, P.G. Newbery, M.G. Jayne: Modelling Fuse Elements using a C.A.D. Software Package. 5th ICEFA, Ilmenau 1995.
- 6 D. de Cogan, M. Henini: TLM Modelling of Thin Film Fuses on Silica and Alumina. 3rd ICEFA, Eindhoven 1987.
- 7 L.A.V. Chepel, A.F. Howe: Calculation of Pre-Arcing Times by Transmission-Line Modelling (TLM). 4th ICEFA, Nottingham 1991.
- 8 M. Hofmann: Experimentelle und rechnerische Untersuchung von Ansprechennlinien und Alterungsvorgängen bei Sicherungsschmelzleitern. Thesis TU Braunschweig 1987.
- 9 M. Hofmann, M. Lindmayer: Precalculation of Time/Current Characteristics of „M“-Effect Fuse Elements. 3rd ICEFA, Eindhoven 1987.
- 10 M. Xian-Zhong, W. Ji-Mei: The Simulation of Prearcing Characteristics of Fuse Elements in the Finite Element Method. 3rd ICEFA, Eindhoven 1987.
- 11 J.C. Gomez, D. Tourn, P.M. McEwan: Investigation of the Pre-Arcing Behaviour of Dissimilar Uniform Double-Elemented Filled Fuses, Using CAD Techniques. 4th ICEFA, Nottingham 1991.
- 12 C. Garrido, J. Cidras: Analysis of Prearcing Time-Current Characteristic of Fuselinks. 4th ICEFA, Nottingham 1991.
- 13 D.A. Beaujean, M.G. Jayne, P.G. Newbery: Determination of M-Effect Diffusion Parameters in High Breaking Capacity Fuses. IEE Proc.-Sci. Meas. Technol., Vol. 142, March 1995, p. 162
- 14 S.V. Patankar: Numerical Heat Transfer and Fluid Flow. Hemisphere Publishing Corporation 1980.
- 15 H. Eckhardt: Numerische Verfahren in der Energietechnik. Teubner Studienskripten, Stuttgart 1978.
- 16 M. Lindmayer: Simulation of Stationary Current-Voltage Characteristics and of Back-Commutation in Rectangular Arc Channels. 17th Int. Conf. on Electrical Contacts, Nagoya 1994.
- 17 D.S. Kershaw: The Incomplete Cholesky-Conjugate Gradient Method for the Iterative Solution of Systems of Linear Equations. Journal of Computational Physics, 26, 1978, pp.43-65.
- 18 H. Fidos, H. Schreiner: Feuerverzinnung von Kupferschaltdrähten, Teil1. Zeitschrift für Metallkunde 61 (1960), pp.225-228.
- 19 S. Øvland, J. Kulsetås, H. Förster, W. Rondeel: Metallurgical Deterioration of Copper Fuse Elements in High Voltage Fuses. 2nd ICEFA, Trondheim 1984.
- 20 M. Hansen: Constitution of Binary Alloys. McGraw-Hill 1958.
- 21 M. Luther: Flinke Hochleistungs-Metallschicht-sicherungen - Experimente und Simulationen. Thesis TU Braunschweig 1993.